

A 150-year Isotopic Record of Lead Deposition in Yancheng Coastal Wetland, China

BAO Kunshan¹, SHEN Ji¹, QUAN Guixiang², LIU Fugang³

(1. State Key Laboratory of Lake Science and Environment, Nanjing Institute of Geography and Limnology, Chinese Academy of Sciences, Nanjing 210008, China; 2. School of Environmental Science and Engineering, Yancheng Institute of Technology, Yancheng 224051, China; 3. School of Science, Qiqihar University, Qiqihar 161006, China)

Abstract: Radioactive markers are useful in dating lead (Pb) deposition patterns from industrialization in sedimentary archives. As a well-known natural reserve in the world, Yancheng coastal wetland in Jiangsu Province is one of areas most sensitive to global sea level change and is located in the most developed and polluted region of China. Two cores were collected in Yancheng wetland in October 2013 and dated using ²¹⁰Pb and ¹³⁷Cs radiometric techniques. Sediments in both cores were sectioned into depth bands and examined systematically for dry bulk density, water content, magnetic susceptibility and grain-size. Multiple elements including Pb were also measured using inductively coupled plasma systems. Unsupported ²¹⁰Pb activities decreased with depth in both of the two cores, and ²¹⁰Pb chronologies were established (covering 150 years) using the constant rate of supply (CRS) model. The measured Pb contents ranged from 14.97 mg/kg to 29.40 mg/kg with average values of 17.17–22.79 mg/kg, and the Pb fluxes ranged from 41.70 mg/(m²·yr) to 172.70 mg/(m²·yr) with averages of 95.59–123.41 mg/(m²·yr). Temporal variations of Pb flux, enrichment factors and Pb isotopes show a gradual and continuous increase over time and clearly reflect increased emissions from anthropogenic activities in the region. The Pb isotopic compositions show that most of Pb deposition in Yancheng wetland is input from natural sources by water flows and has the same levels of Pb as in the surface sediment of the Yangtze River and the Pacific mineral aerosol. We also stress the anthropogenic Pb contribution in Yancheng wetland sediment and the reason of our Pb isotopes not showing anthropogenic signature is likely the instability of anthropogenic Pb in high Fe/Mn oxide conditions. Therefore, more attention should be paid to current local pollution problems, and society should take action to seek a balance between economic development and environmental protection.

Keywords: coastal wetland; Pb deposition rate; Pb isotope; ²¹⁰Pb dating; metal pollution

Citation: Bao Kunshan, Shen Ji, Quan Guixiang, Liu Fugang, 2016. A 150-year isotopic record of lead deposition in Yancheng coastal wetland, China. *Chinese Geographical Science*, 26(6): 755–769. doi: 10.1007/s11769-016-0835-9

1 Introduction

Coastal wetlands are ecosystems which exist within an elevation gradient ranging between the landward edge where the sea passes its hydrologic influence to groundwater and atmospheric processes and subtidal depths to which light penetrates to support photosynthe-

sis of benthic plants (Perillo *et al.*, 2009). They are complex and diverse including salt marshes, mangroves, tidal flats, and sea grasses, and thus rank among the most productive of all natural ecosystems (Leorri *et al.*, 2013). As one of the most significant ecosystems in the world, the coastal wetlands have many intrinsic values, including high resilience against extreme weather, wide

Received date: 2015-06-25; accepted date: 2015-10-18

Foundation item: Under the auspices of Natural Science Foundation of Jiangsu Province, China (No. BK20131058), NSFC-CNRS (National Natural Science Foundation of China-Centre National de la Recherche Scientifique (National Center for Scientific Research)) Joint Research Project (No. 41611130163), National Natural Science Foundation of China (No. 41301215) and National Basic Research Program of China (No. 2012CB956100)

Corresponding author: BAO Kunshan. E-mail: ksbao@niglas.ac.cn

© Science Press, Northeast Institute of Geography and Agroecology, CAS and Springer-Verlag Berlin Heidelberg 2016

variety of plant and animal species, and significant social-economic benefits to fisheries (Pennings, 2012). Coastal wetland regions have been attractive sites for human settlement over several millennia, and continued population growth and increasing global food demand lead to conversion of around 25%–50% of the world's coastal wetlands into farmland and aquafarms (Regnier *et al.*, 2013). In addition, anthropogenic contamination has been increasing, particularly due to land use change, discharge of sewage from urban areas and industrial emissions over the past decades (Monteiro *et al.*, 2012). Among pollutants released to the coastal environments by such human activities, heavy metals are the most persistent and have received extensive attention over the world (Jayaprakash *et al.*, 2010; Mahiques *et al.*, 2013).

Lead (Pb) has the highest fraction of anthropogenic components among all trace metals, and is the most representative of heavy metals adversely affecting the global environment (Bao *et al.*, 2010). Pb is often used as marker of historical environmental changes to evaluate the anthropogenic influence, largely because it is not subjected to significant post-depositional migration before or after entering into the sediments (Molisani *et al.*, 2004; Zohar *et al.*, 2014). Therefore, much research on the potential of sedimentary cores from coastal wetlands as archives of anthropogenic Pb pollution has been carried out worldwide (Deely and Fergusson, 1994; Perkins *et al.*, 2000; Chan *et al.*, 2001; Connor and Thomas, 2003; Zourarah *et al.*, 2007; Hosono *et al.*, 2010; Mahiques *et al.*, 2013; Zohar *et al.*, 2014). Exact dating of core sections is essential for the reconstruction of the Pb deposition history from coastal wetlands (Kim *et al.*, 2004). Short-lived radioisotopes such as ^{210}Pb (half-life 22.3 years) have been used to document recent (past 200 years or less) atmospheric metal deposition in coastal sediments (DeLaune *et al.*, 1978; Church *et al.*, 1981; Sharma *et al.*, 1987; Zwolsman *et al.*, 1993; Kim *et al.*, 1997). In order to obtain a reliable age in dating sediments, measurements of stable Pb isotopes are often applied to check the ^{210}Pb chronologies based on the transient history of $^{206}\text{Pb}/^{207}\text{Pb}$ ratios during the 20th century (Kim *et al.*, 2004). For example, the phase-out of leaded gasoline in China started in the 1990s, with leaded gasoline being banned in several major cities (i.e., Beijing and Shanghai) in 1997 and 1998, and nationwide in 2000 (Cheng and Hu, 2010), and thus the $^{206}\text{Pb}/^{207}\text{Pb}$ ratios would present a shift towards much

more radiogenic values. Furthermore, the stable Pb isotopic compositions have been useful in characterizing and distinguishing between anthropogenic and natural sources (Patterson and Settle, 1987; Kim *et al.*, 1997; Wang *et al.*, 2014). Anthropogenic Pb in China results from the combustion of fossil fuel, mining and smelting, electronic waste recycling, municipal solid waste incineration, landfills, Pb paint and other industrial sources (Flegel *et al.*, 2013). Due to a sharp increase of coal consumption since 2003, it was reported that atmospheric Pb emissions had changed in the last two decades in China and the coal combustion and non-ferrous metal smelting were the dominant emission sources (Li *et al.*, 2012).

In China, meeting future food and energy demands while mitigating the potential detrimental environmental impacts has emerged as one of the greatest challenges in exploitation and conservation of coastal wetlands (Kirwan and Megonigal, 2013). For example, the tidal flats in north Jiangsu Province are the largest coastal wetlands in China and are world-renowned habitats for many rare and endangered plant and animal species. Although two wetland reserves of international importance have been established, the Dafeng National Nature Reserve (Ramsar site no. 1145) and the Yancheng National Nature Reserve (YNNR, Ramsar site no. 1156), the outlook for broader protection is not optimistic. From 1988 to 2006, the decrease rate of the grass flat in YNNR was ca. 900 ha/yr, and the increase rate of the farmland and pond areas were ca. 600 ha/yr and 1400 ha/yr (Ke *et al.*, 2011). This is not an isolated case in China; it has been reported that 57% of China's coastal wetlands have disappeared due to land reclamation since the 1950s (Qiu, 2011).

Therefore, the objectives of this study were to reconstruct the historical deposition of Pb through two ^{210}Pb and ^{137}Cs dated sediment cores from the Yancheng coastal wetland of north Jiangsu Province, China, and to investigate its potential sources and links with the development of industries through Pb isotopic signatures. This study would be helpful to reveal the anthropogenic effects on regional environment and to provide support for policy-making in sustainable development.

2 Materials and Methods

2.1 Study area

The coastal region in Yancheng City of Jiangsu Province

faces the Yellow Sea to the east and the Yangtze River to the south. The Yancheng wetlands cover a total area of 4530 km² (ca. 30% of the municipality's total area), in which the supratidal zone occupies an area of 1673 km², the intertidal zone occupies an area of 1613 km², and the other is radial sand ridges, accounting for 70% of the provincial total and 14.3% of the national total. They consist primarily of extensive inter-tidal mudflats, tidal creeks and river channels, salt marshes, reed beds and marshy grasslands that provide desirable habitats for numerous species of plant and animal of national and global importance. Moreover, the wetlands provide important ecosystem services to local communities, and also improve water quality by assimilating some of the household and industrial wastes that are rapidly increasing in Yancheng City. The Yancheng wetlands have been listed in the world network of biosphere conservation (WBNP) by the United Nations since 1992, and have become the hotspot of wetland research for their significance. However, the Yancheng coastal wetland has been experiencing rapid degradation due to the rapid economic development and frequent land use changes. Human-induced land use along this coastal region in-

cludes mainly agriculture, aquaculture, and solar salt production. In recent times, human activities of harbor building, wind power generation, and tourism have increased. The associated sewage and solid wastes are also increasing (Chuai et al., 2014).

The sampling site is situated in Sheyang County of Yancheng City (Fig. 1), which belongs to Yancheng coastal wetland. At present, the wetland landscape from sea to land shows ecological zones of the bare silt-sand mixed flats, the *Spartina alterniflora* flat, the *Suaeda salsa* flat and the *Phragmites australis* flat (Gao et al., 2012). This wetland is located in the north subtropical zone with average precipitation of 1010 mm/yr and annual average temperature of 14.4°C. The tidal flat is affected by the marine monsoon climate with prevailing southeastern wind in summer and prevailing northwestern wind controlled by tropical depression in winter (Liu et al., 2010). This site is a plain sedimentary geomorphology (average slope: 0.055%) formed by the fluvial and coast sedimentary processes since the end of the late Pleistocene. The soils are classified as Anthrosols, Fluvisols, and Cambisols according to the formation process (Fang et al., 2010).

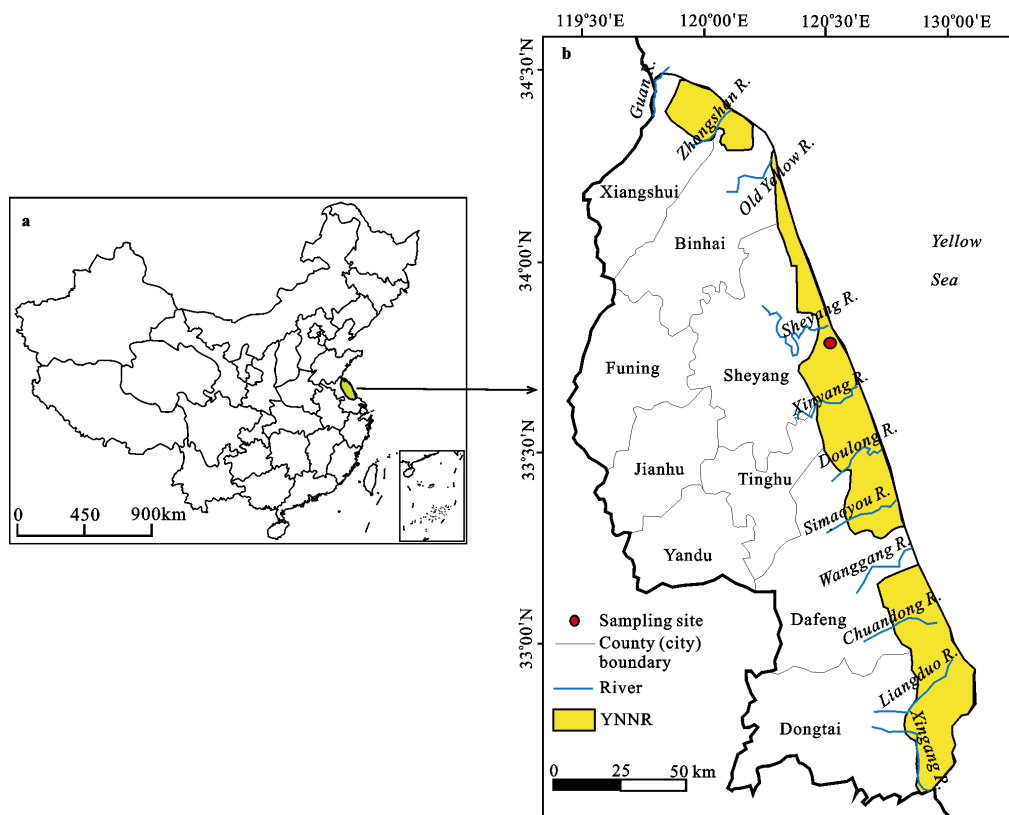


Fig. 1 China map showing location of Yancheng City in Jiangsu Province (a) and Yancheng map showing Yancheng National Nature Reserve (YNNR) and sampling site (b)

2.2 Core-sampling and slice-sectioning

Two sediment cores were collected using a motorized corer (Eijkelpamp, Netherlands) from the *S. alterniflora* flat (labeled SAF-1, 33°46'34"N, 120°31'49"E, altitude 3 m) and the bare flat (labeled BAF-1, 33°44'37"N, 120°31'50"E, altitude 1 m) in October 2013 (Fig. 2). The latitude, longitude, and altitude at sampling sites were determined with a portable global positioning system (Garmin GPS 62SC, Garmin International, Olathe, KS). The cores were taken back to the laboratory, and split longitudinally. One-half was archived in the frozen condition and the other half was precisely cut into 1 cm slices using a stainless steel semi-circular blade of the same diameter as the core tube. All slices were packed into labeled zip-lock polyethylene plastic bags for storage and further preparation.

2.3 Physical and chemical analysis

Water content (%) and dry bulk density (DBD, g/cm³) of the samples were determined by weighing the 1 cm slices of the sediment cores before and after freeze drying overnight. Mass magnetic susceptibility was quantified from the homogenized, dried samples using a MS2

sensor (Bartington Instruments Ltd, Oxford, UK). Particle size spectra were determined using a Malvern automated laser-optical particle-size analyzer (Master-sizer-2000; Malvern Instruments Ltd, Worcestershire, UK) after removal of organic matter by 10% hydrogen peroxide treatment. This instrument has a measurement range of 0.02–2000 μm and an error of less than 3% with repeated measurements.

2.4 Determination of age using ²¹⁰Pb and ¹³⁷Cs

Bulk weighed dry samples were sealed in plastic test tubes with caps for subsequent ²¹⁰Pb dating by gamma spectrometry with well-type coaxial low background intrinsic germanium detectors (Ortec HP Ge GWL series, Oak Ridge, TN, USA). Radioactivity levels of ²¹⁰Pb were determined via gamma emissions at 46.5 keV. Emissions of ²²⁶Ra with the 295 keV and 352 keV γ-rays emitted by its daughter nuclide ²¹⁴Pb were determined after 3 weeks storage in sealed containers to allow radioactive equilibrium. Radioactivities of ¹³⁷Cs were measured with the 662 keV photo peak. Standard sources and sediment samples of known activity were provided by China Institute of Atomic Energy and used

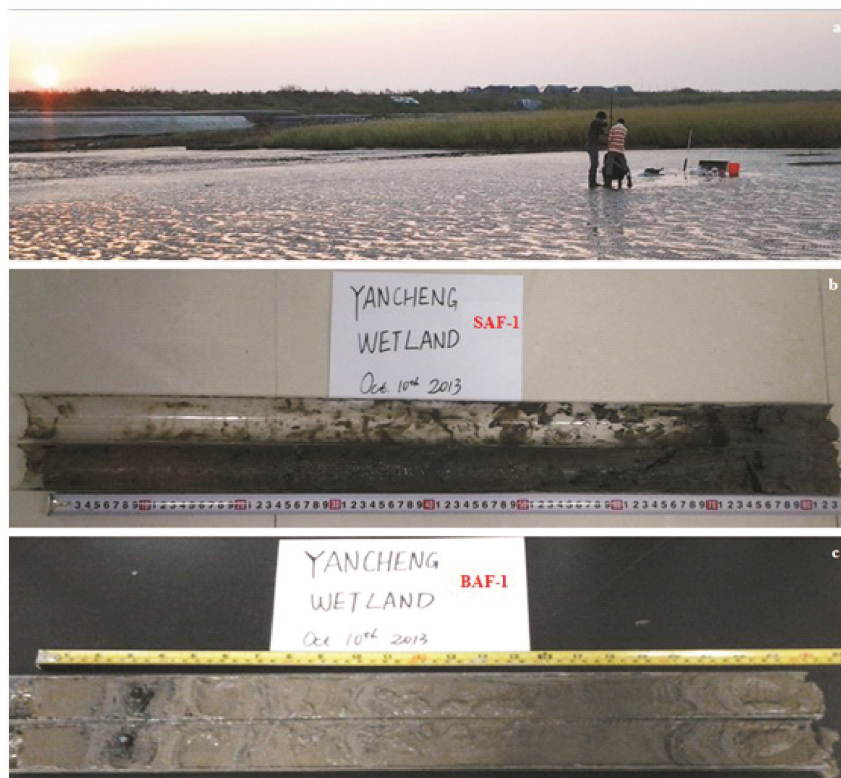


Fig. 2 A photo showing sampling site scene at Yancheng coastal wetland and core sampling in the field (a), and photos showing the sediment cores of SAF-1 (b) and BAF-1 (c) that PVC pipes were cut in half to show the lithologic character in laboratory

to calibrate the absolute efficiencies of the detectors. Counting times of ^{137}Cs and ^{210}Pb were typically in the range 50 000–86 000 s, giving a measurement precision of between $\pm 5\%$ and $\pm 10\%$ at the 95% level of confidence, respectively. Supported ^{210}Pb in each sample was assumed to be in equilibrium with the in-situ ^{226}Ra , and unsupported ^{210}Pb activities were determined from the difference between the total ^{210}Pb and the supported ^{210}Pb activity.

2.5 Analysis of Pb content and isotopes

Twenty-eight elements were measured by an Atomic Emission Spectroscopy with Inductively Coupled Plasma (ICP-AES Prodigy7, Teledune Leeman Labs, USA) and a Quadrupole Inductively Coupled Plasma Mass Spectrometry (Q-ICP-MS 7700x, Agilent Technologies, USA) (unpublished data). Of these, only aluminium (Al), manganese (Mn), iron (Fe), and Pb and its stable isotopes (^{206}Pb , ^{207}Pb , ^{208}Pb) were used in this study. The contents of Al were applied to quantify the natural “background” or lithogenic component for calculation of enrichment factor of Pb. The contents of Mn and Fe were applied to evaluate the redox state of the samples. The digestion procedure for elemental analyses is as follows.

Sample aliquots were dried at 105°C for 12 h and ground using an agate mortar. The ground sample was weighed accurately (0.2000–0.2059 g) into a TFM-PTFE liner vessel (bomb) with the stainless steel pressure digestion system (DAB-2, Berghof, Berchtesgaden, Germany). Then, 2.5 mL HNO_3 (high purity obtained by sub-boiling distillation of the analytical-grade reagent in an I.R. distiller (BSB-939, Berghof, Berchtesgaden, Germany)) and 0.5 mL H_2O_2 (Baker ACS Reagent) were added and the PTFE vessels were closed and heated at $200\text{--}220^\circ\text{C}$ for 3 h. After cooling, 1 mL HF (Baker ACS Reagent) and 0.5 mL HClO_4 (Fisher Trace Metal Grade)

were added and they were heated again until the white smoke from the liner disappeared. After cooling again, 0.5 mL HNO_3 (high purity) and 2.5 mL deionized water ($> 18 \text{ M}\Omega\cdot\text{cm}$) were added and they were heated at $150\text{--}180^\circ\text{C}$ for 5 min. Finally, they were cooled to ambient temperature for a minimum of 2 h, and the digested samples were transferred to a 50 mL centrifuge tube along with the washings from the TFM-PTFE liner. The sample solutions were brought up to a final volume of 25 mL with deionized water for elemental analyses. The above solutions were diluted to a concentration of $8\text{--}10 \mu\text{g/L}$ Pb for measuring the isotopic composition of Pb (Mihaljevič *et al.*, 2006).

For quality control, a reference standard consisting of stream sediments (GBW07358, Institute of Geophysical and Geochemical Exploration, Langfang, China) was included after every five samples during the elemental measurement process. Average measured contents of Al, Mn, Fe and Pb for the reference materials, and their respective values measured independently by Institute of Geophysical and Geochemical Exploration are given in Table 1. The limit of detection (LOD) is given as three times the relative standard deviation (RSD) of three blind replicates. The RSD for $^{206}\text{Pb}/^{207}\text{Pb}$ and $^{208}\text{Pb}/^{206}\text{Pb}$ is $< 0.12\%$ and $< 0.07\%$, respectively.

2.6 Calculation of chronology, flux and enrichment factor

Due to tidal and anthropogenic effects which result in varying sedimentary rates, the core chronology was determined using constant rate of supply (CRS) dating model (Appleby, 2008) according to Equation (1). Sediment rate (SR, cm/yr) was calculated based on the ^{210}Pb inferred chronologies according to Equation (2) (Bao *et al.*, 2010). To estimate inventories, burial fluxes of sediment mass and anthropogenic Pb components in the sediment cores of a given area, several sediment

Table 1 Analytical result for element contents in reference material (Stream sediments GBW07358)

| Metal | Measured value | | | | Certified value | LOD ^a |
|------------|----------------|---------|----------------|--------------------|------------------|------------------|
| | Minimum | Maximum | Mean ($n=3$) | Standard Deviation | | |
| Al (mg/g) | 57.50 | 58.10 | 57.73 | 0.32 | 58.54 \pm 0.69 | 0.01 |
| Fe (mg/g) | 46.10 | 47.20 | 46.50 | 0.61 | 48.96 \pm 0.70 | 0.002 |
| Mn (mg/kg) | 1396.00 | 1416.00 | 1407.30 | 10.26 | 1420 \pm 40 | 0.5 |
| Pb (mg/kg) | 208.00 | 213.00 | 211.00 | 2.65 | 210 \pm 6 | 0.02 |

Note: a, LOI represents limit of detection

properties including DBD, SR and the sediment porosity (SP, dimensionless) must be taken into account in addition to the sediment mass and Pb content. SP was defined as one minus the ratio of DBD and the solid-grain density (SGD) which was taken as 2.7 g/cm^3 (Baldwin and Butler, 1985) according to Equation (3). Mass accumulation rate (MAR, $\text{g}/(\text{cm}^2\cdot\text{yr})$) and the Pb burial flux ($\text{mg}/(\text{cm}^2\cdot\text{yr})$) were estimated by the equations (4) and (5) (Bao *et al.*, 2015a). As an approach to characterize variation of elemental content in the sediments, the Pb enrichment factor (Pb EF) relative to the Earth's Upper Continental Crust (UCC) was calculated according to Equation (6) (Bao *et al.*, 2015b) and used to indicate the anthropogenic contribution to Pb accumulation in the sediments.

$$T_Z = -(1/\lambda)\ln(I_Z/I_{\text{tot}}) \quad (1)$$

$$SR_Z = Z / T_Z \quad (2)$$

$$SP = 1 - DBD / SGD \quad (3)$$

$$MAR = DBD \times SR_Z \times (1 - SP) \quad (4)$$

$$Pb \text{ Flux} = Pb \times DBD \times SR_Z \times (1 - SP) \times 10 \quad (5)$$

$$Pb \text{ EF} = (Pb/Al)_{\text{sample}} / (Pb/Al)_{\text{UCC}} \quad (6)$$

where T_Z (yr) is the age of layer at depth Z (cm); I_Z and I_{tot} refer to the inventory of unsupported ^{210}Pb at depth Z (cm) and the total inventory of unsupported ^{210}Pb in the core section (both are calculated by direct numerical integration); λ is the ^{210}Pb decay constant ($0.0311/\text{yr}$); SR_Z is the sediment rate at depth Z (cm); and the number, 10 in Equation (5) is a unit conversion factor.

2.7 Data statistical analysis

Values of mean, standard deviation, minimum and maximum were calculated for the core parameters. All data were converted to Z -scores calculated according to Equation 7 before regression analysis which was performed to examine the relationships among the individual parameters. Statistical significance was determined at the $p = 0.05$ level except if indicated differently. These procedures were performed using SPSS 11.5 software package (SPSS, 2002).

$$Z_{\text{-score}} = (X_i - X_{\text{avg}}) / X_{\text{std}} \quad (7)$$

where X_i , X_{avg} , and X_{std} are the measured value, the average and the standard deviation respectively of the i th variable in a sample.

3 Results

3.1 Physicochemical properties of sediment

Water content of both SAF-1 and BAF-1 cores ranged from 20%–40%. The distributions were similar for the two cores and characterized by the highest value occurring at the near surface sections, with a general decrease at the deeper layers (Fig. 3a). However, a peak-valley pattern of water content with depth for both cores was observed, which probably reflected the periodical variation of ground water level that is mainly affected by the sea water level. Dry bulk density of SAF-1 core ranged from 0.75 g/cm^3 to 1.45 g/cm^3 , and that of BAF-1 core ranged from 1.07 g/cm^3 to 1.52 g/cm^3 (Fig. 3b). The DBD of SAF-1 showed an obvious increase with increasing depth. The pattern of DBD below ca. 20 cm was similar for both cores. Lower DBD values of SAF-1 than BAF-1 for the topmost sections were likely a result of the existence of vegetation in SAF-1; the top layer of the sediment in SAF-1 was black and contained a large content of decayed *S. alterniflora*. Variations of mass magnetic susceptibility for the two cores were quite similar with elevated levels in the upper layers of the profiles (Fig. 3c). Profiles of grain-size variation with depth in the two cores are shown in Fig. 3. The grains were divided into the following size groups: sand ($> 64 \mu\text{m}$), silt ($4\text{--}64 \mu\text{m}$) and clay ($< 4 \mu\text{m}$). The clay fraction ranged from 5.4% to 33.4% (with a mean of 16.3%) for SAF-1 and from 8.4% to 19.2% (with a mean of 12.8%) for BAF-1 (Fig. 3d); silt content ranged from 60.8% to 82.2% (with a mean of 73.1%) for SAF-1 and from 56.8% to 78.7% (with a mean of 70.7%) for BAF-1 (Fig. 3e); sand content ranged from 1.2% to 27.9% (with a mean of 10.6%) for SAF-1 and from 8.6% to 25.7% (with a mean of 16.5%) for BAF-1 (Fig. 3f). They fluctuated within a certain range in the two cores, and the silt particles were the dominant component.

3.2 Radioisotope chronology and sediment rate

Radioisotope results for ^{210}Pb are plotted in Fig. 4a and c for the two cores. Their unsupported ^{210}Pb activities (excess ^{210}Pb , $^{210}\text{Pb}_{\text{exe}}$) presented a relatively well-defined logarithmic decrease with depth and they became negligible at the bottom of both cores because the total ^{210}Pb is in equilibrium with ^{226}Ra (^{214}Pb). The continuous ages were calculated using the CRS dating model and the age-depth models for both cores were

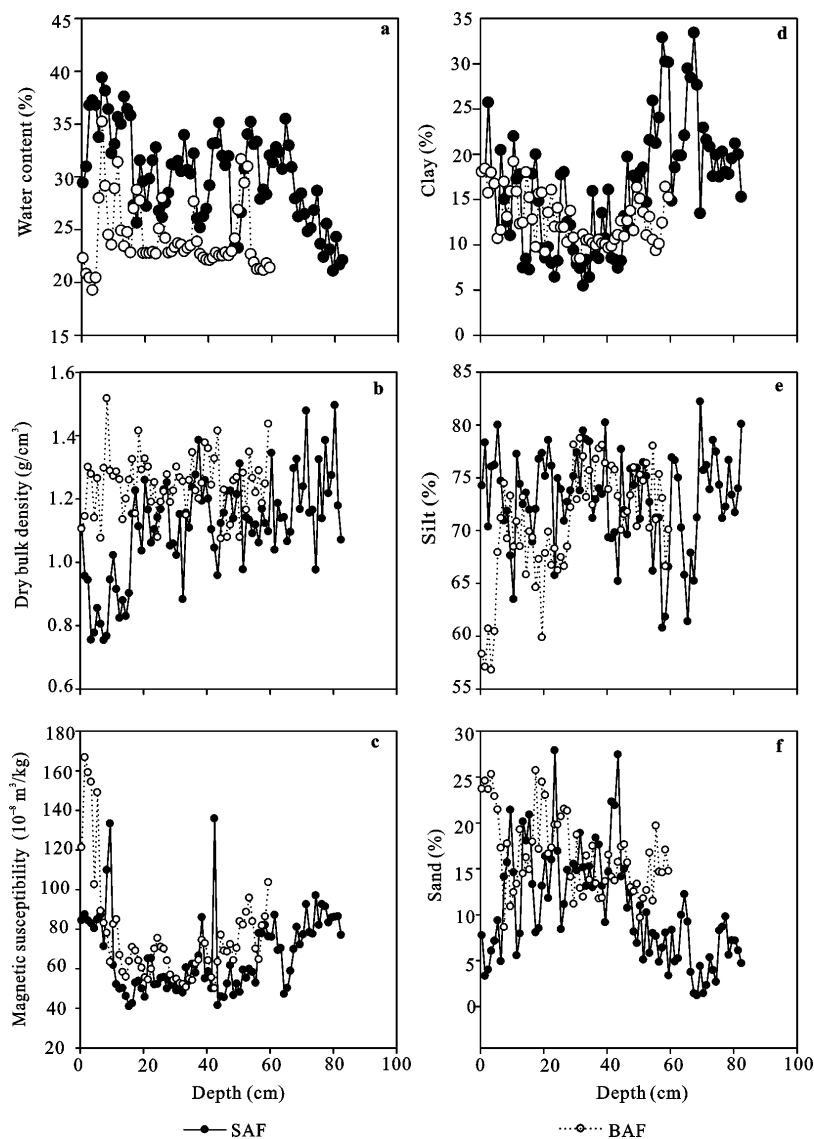


Fig. 3 Depth variations of water content (a), dry bulk density (b), mass magnetic susceptibility (c), and grain-size composition (clay, d; silt, e; sand, f) of two sediment cores (SAF-1 and BAF-1) in Yancheng coastal wetland, China

plotted (Fig. 4b and d). The sediment records cover about 150 years for SAF-1 and 125 years for BAF-1, reaching back to 1860 AD and 1885 AD, respectively. The ^{137}Cs activity for both cores was relatively low along the entire profiles. The maximum activities of ^{137}Cs were 1.22 Bq/kg at depth of 20 cm for SAF-1 and 1.72 Bq/kg at depth of 46 cm for BAF-1. The substantial difference in depth for the maximum ^{137}Cs activities in the two cores indicates that the ^{137}Cs technique did not provide a reliable chronostratigraphic index in our sediment samples. This is likely because ^{137}Cs was not well preserved in silt-fine sand and mud-sand sediments

of Yancheng coastal wetland. Consequently, the results of ^{137}Cs activities were not used to check the date in this study. From the ^{210}Pb -derived age, the calculated SR of SAF-1 core ranged from 0.54 cm/yr to 1.70 cm/yr, with an average of 1.28 cm/yr, and that of BAF-1 core ranged from 0.47 cm/yr to 1.14 cm/yr, with an average of 0.93 cm/yr (Fig. 5a). MAR of both cores ranged from 0.24 g/(cm²·yr) to 0.84 g/(cm²·yr) with an average of 0.55 g/(cm²·yr) (Fig. 5b). The overall patterns were quite similar for both cores, with a general increasing trend over time reaching a maximum value around 2000 AD and then a decrease afterwards.

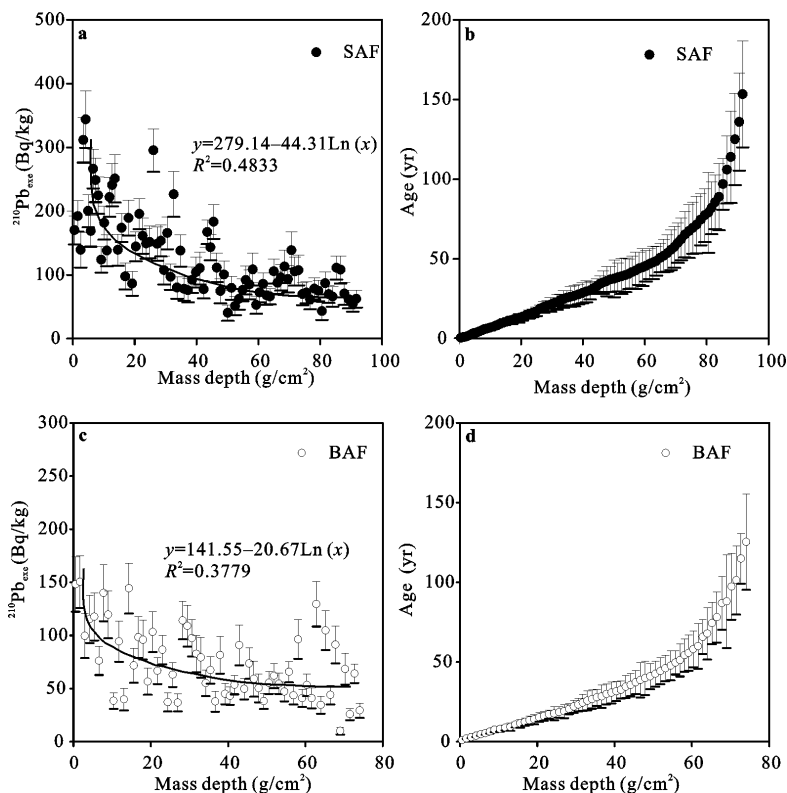


Fig. 4 ^{210}Pb activity and ^{210}Pb -inferred chronologies plotted against mass depth for SAF-1 core (a and b) and BAF-1 core (c and d). Error bars represent standard deviation (SD) from counting uncertainty

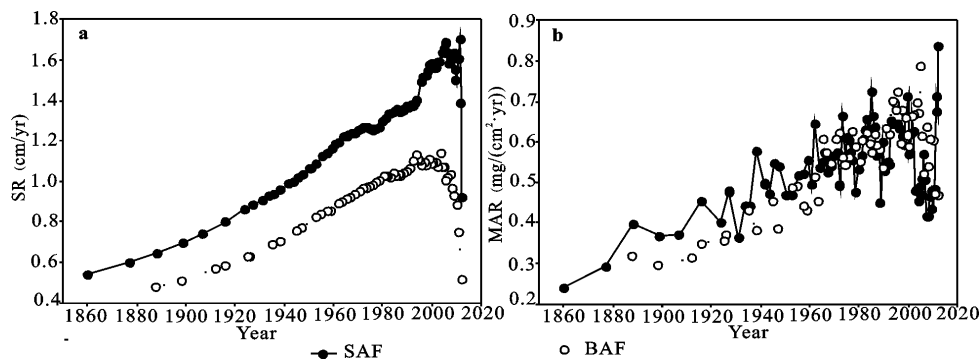


Fig. 5 Sediment rate (SR) and mass accumulation rate (MAR) plotted against age determined from ^{210}Pb (calendar year AD) of two sediment cores (SAF-1 and BAF-1) in Yancheng coastal wetland, China

3.3 Elemental contents and Pb isotopes

The measured elemental contents of Al, Mn, Fe, Pb and Pb isotopic ratios are summarized in Table 2. The average values of Al, Mn, Fe and Pb were 64 mg/g, 732.7 mg/kg, 32 mg/g and 22.79 mg/kg for SAF-1, and 56 mg/g, 514.7 mg/kg, 26 mg/g and 17.17 mg/kg for BAF-1, respectively. The Pb isotopes showed a narrow variation, with relatively stable averages of $^{206}\text{Pb}/^{207}\text{Pb}$ (1.1942 ± 0.0034 for SAF-1 and 1.1963 ± 0.0064 for BAF-1) and $^{208}\text{Pb}/^{206}\text{Pb}$ (2.0868 ± 0.0022 for SAF-1 and 2.0875 ± 0.0024 for BAF-1). Depth variations of meas-

ured elemental contents and Pb isotopic ratios were consistent for the two cores and showed several obvious peaks (Fig. 6).

4 Discussion

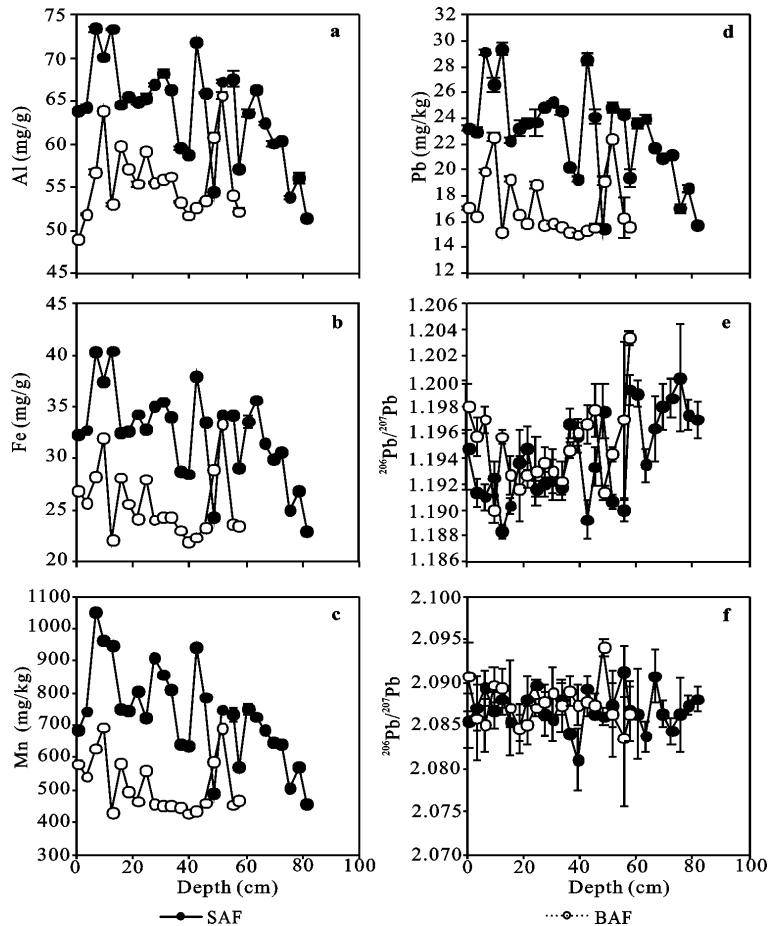
4.1 Characteristics of depositional environment

The sedimentary historical information on environmental changes within the coastal areas could have been disturbed by the interactions between the land and the ocean. An effective way was suggested to track the

Table 2 Maximum, minimum and mean elemental contents and Pb isotopic ratios with standard deviation (SD) based on numbers of samples for each profile

| | Number | Minimum | Maximum | Mean | SD |
|-----------------------------------|--------|---------|---------|--------|--------|
| SAF-1 | | | | | |
| Al (mg/g) | 28 | 51.40 | 73.40 | 63.69 | 5.72 |
| Mn (mg/kg) | 28 | 457.00 | 1052.33 | 732.68 | 146.91 |
| Fe (mg/g) | 28 | 23.00 | 40.40 | 32.37 | 4.37 |
| Pb (mg/kg) | 28 | 15.47 | 29.40 | 22.79 | 3.60 |
| $^{206}\text{Pb}/^{207}\text{Pb}$ | 28 | 1.1883 | 1.2003 | 1.1942 | 0.0034 |
| $^{208}\text{Pb}/^{206}\text{Pb}$ | 28 | 2.0810 | 2.0913 | 2.0868 | 0.0022 |
| BAF-1 | | | | | |
| Al (mg/g) | 20 | 49.00 | 65.63 | 55.86 | 4.24 |
| Mn (mg/kg) | 20 | 425.67 | 693.00 | 514.70 | 86.45 |
| Fe (mg/g) | 20 | 21.90 | 33.37 | 25.66 | 3.22 |
| Pb (mg/kg) | 20 | 14.97 | 22.57 | 17.17 | 2.36 |
| $^{206}\text{Pb}/^{207}\text{Pb}$ | 20 | 1.1900 | 1.2180 | 1.1963 | 0.0064 |
| $^{208}\text{Pb}/^{206}\text{Pb}$ | 20 | 2.0835 | 2.0940 | 2.0875 | 0.0024 |

depositional environment by integrating the physico-chemical parameters and the isotope dating (Liu *et al.*, 2013). Here we obtained water content, bulk density, grain-size and magnetic susceptibility to characterize the depositional processes. Our results of water content are consistent with a previous report for the bare silt zone (average 30%, the whole core of 120 cm) and for the *S. alterniflora* zone (average 40%, the lower 20–120 cm section and significantly elevated in the surface 20 cm) in this same coastal wetland (Gao *et al.*, 2012). The grain-size distribution reflects that this region is the silt-fine sand and mud-sand mixed tidal flat, which was well known (Liu *et al.*, 2010; Li and Gao, 2013). It is worthy to note that the coarse particles in vegetated flat (i.e., SAF-1) were less than the bare flat (i.e., BAF-1) (Fig. 3), which was attributed to the trapping effect where plants obstruct tidal flow (Liu *et al.*, 2013; Gao *et al.*, 2014). In addition, the plant residue decomposition also contributed to the accumulation of fine particles in

**Fig. 6** Depth variations of measured elemental contents and Pb isotopic ratios ($^{206}\text{Pb}/^{207}\text{Pb}$ and $^{208}\text{Pb}/^{206}\text{Pb}$) of two sediment cores (SAF-1 and BAF-1) in Yancheng coastal wetland, China. Error bars represent the standard deviation (SD) of the mean of three parallel samples

the sediments. Magnetic susceptibility is directly linked to a concentration of anthropogenic ferromagnetic particles and is dominated by high values of magnetite produced during the combustion of fossil fuel (Kapička *et al.*, 1999). The pattern of mass magnetic susceptibility confirmed that our study area was severely contaminated by industrial activities. The average SR is approximately consistent with the rate of 1.2 cm/yr on Xingyanggang tidal flat (Liu *et al.*, 2010), which is only 15 km distant from our study site, but smaller than the rate of 3.0 cm/yr on Wanggang salt marsh, which is about 75 km southeast of our study site (Wang *et al.*, 2005).

4.2 Historical trend of Pb enrichment factor and flux

The measured Pb contents in Yancheng coastal wetland sediments (maximum 29.40 mg/kg) are lower than the baseline of the first class soil (35 mg/kg) according to Environmental Quality Standard for Soils in China (GB15618-1995, 1997). Through correlation analyses, we found there were significant relations between Pb and elements of Al, Mn and Fe ($R^2 > 0.9$, Fig. 7). As a result, we chose Al as a reference element which is the second most abundant element in the Earth's crust and is not significantly influenced by diagenetic process and anthropogenic inputs (Di Leonardo *et al.*, 2014). Calculated enrichment factors of Mn, Fe and Pb for the SAF-1 and BAF-1 cores are shown in Fig. 8. Values of Pb EF of both cores were significantly larger than 1.5, values of Fe EF were slightly greater than 1.0, but values of Mn EF were lower than 1.0. This suggests an enrichment effect of Pb over the whole core and a Pb pollution history in Yancheng region throughout 1860 to 2013. The Pb AR of both cores also had an increasing trend over the past 150 years (Fig. 9a). The Pb AR of SAF-1 ranged from 41.70 mg/(m²·yr) to 172.70 mg/(m²·yr) with an average of 123.41 mg/(m²·yr), and the corresponding value of BAF-1 ranged from 48.22 mg/(m²·yr) to 153.05 mg/(m²·yr) with an average of 95.59 mg/(m²·yr). Yancheng coastal wetland is located in the developed region of China, so the anthropogenic pollutant emissions are severe from residential, industry, transportation, power generation and agricultural waste burned in fields. Therefore, economic and environmental indicators of gross domestic product (GDP), gross industrial production, total energy consumption

and total sown area (Jiangsu Provincial Bureau of Statistics, 2013) and total carbon emission (1995–2010) (Song *et al.*, 2015) in Jiangsu Province were used to assess changes in anthropogenic sources over time (Fig. 10). The increase of energy consumption accompanying the rapid economic development period over the last 20

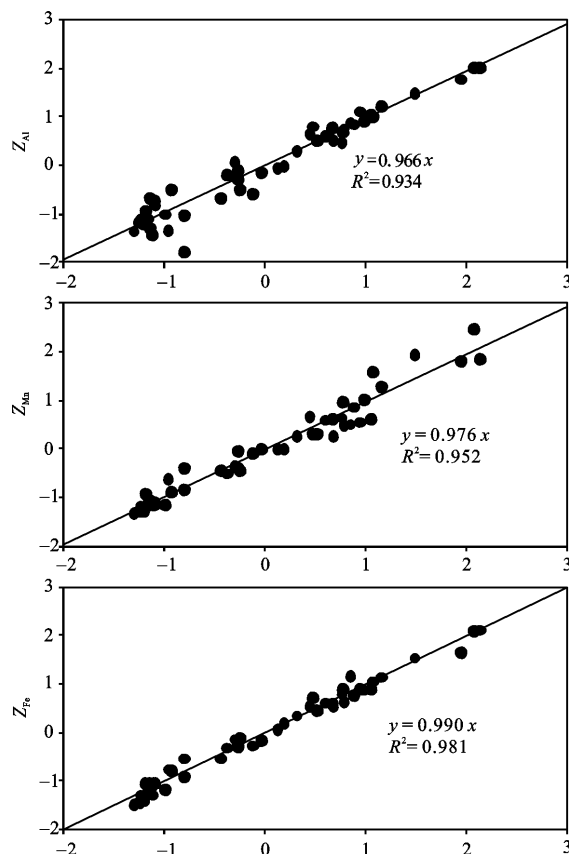


Fig. 7 Correlations between Pb and other elements (Al, Mn and Fe) for two cores from Yancheng coastal wetland, China ($n = 48$)

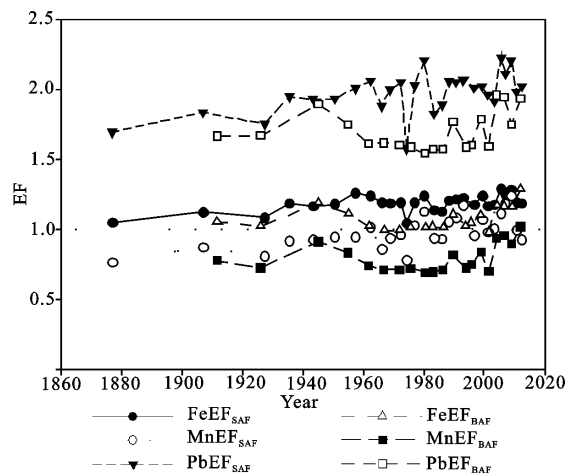


Fig. 8 Enrichment factors (EF) of Mn, Fe and Pb in two cores from Yancheng coastal wetland, China

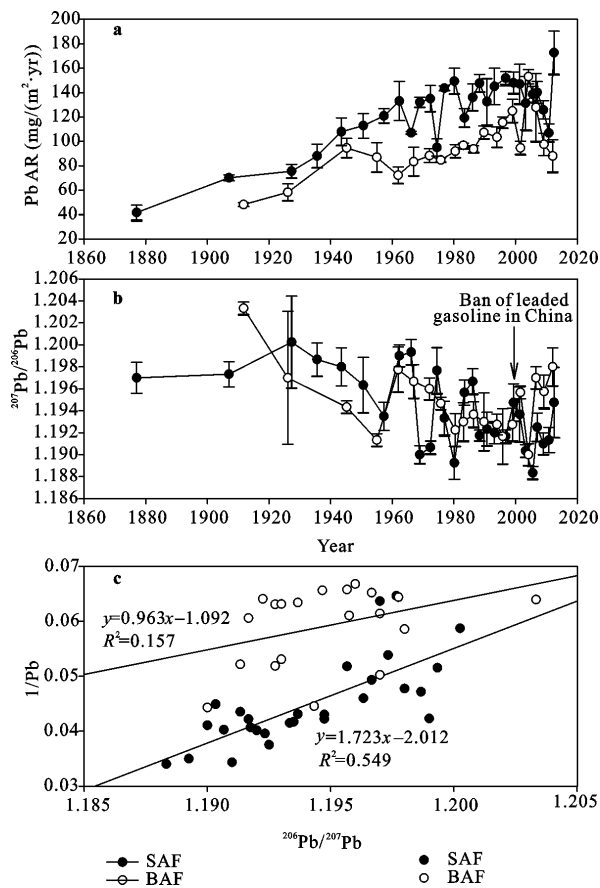


Fig. 9 Temporal variation of accumulation rate (AR) of Pb (a) and $^{206}\text{Pb}/^{207}\text{Pb}$ (b) for the two cores from Yancheng coastal wetland, China, and diagram of $^{206}\text{Pb}/^{207}\text{Pb}$ versus $1/\text{Pb}$ (c). They exhibit significant correlations and the large amount of Pb correspond to the lower $^{206}\text{Pb}/^{207}\text{Pb}$

years corresponds to the trend of increasing Pb flux. This suggests a correlation of anthropogenic sources associated with Pb accumulation in the wetland sediment.

4.3 Sourcing Pb pollution by Pb isotopic ratio

The temporal variations of $^{206}\text{Pb}/^{207}\text{Pb}$ ratio are shown in Fig. 9b, and exhibit a clear decreasing trend with time. The diagram of $^{206}\text{Pb}/^{207}\text{Pb}$ versus the ratio of 1 with Pb ($1/\text{Pb}$) also exhibits significant correlations ($R^2 = 0.549$ for SAF-1 and 0.157 for BAF-1) and the large amount of Pb corresponds to the lower $^{206}\text{Pb}/^{207}\text{Pb}$ (Fig. 9c). As a result, a history of Pb pollution over the past 150 years in Yancheng wetland is constructed, with the highest content of Pb found in recent sediments and associated with less radiogenic (more contaminated) values of $^{206}\text{Pb}/^{207}\text{Pb}$ ratios. The phase-out of leaded gasoline in China started in the 1990s, with leaded gasoline being

banned in several major cities (i.e., Beijing and Shanghai) in 1997 and 1998, and nationwide in 2000 (Cheng and Hu, 2010). This transition is fingerprinted in our temporal variation of $^{206}\text{Pb}/^{207}\text{Pb}$ where it began to increase since ca. 2003 (Fig. 9b).

To visually determine the relative contribution of various potential sources of Pb accumulation in Yancheng coastal wetland, $^{206}\text{Pb}/^{207}\text{Pb}$ versus $^{208}\text{Pb}/^{206}\text{Pb}$ were plotted for all samples and relevant end-members in Fig. 11. Lead isotopic signatures for Pacific mineral aerosols (Jones *et al.*, 2000), Granite, volcanic rocks and uncontaminated soils in China (Lee *et al.*, 2007) are included as proxies of natural sources. Values of coal used in Shanghai (Zheng *et al.*, 2004), vehicle exhaust particles and polluted air, soil and water in Nanjing (Luo *et al.*, 2014) are also included as proxies of anthropogenic sources. For comparison, signatures in the surface sediment of the Yangtze River are also plotted (Choi *et al.*, 2007; Zhang *et al.*, 2008). Taken together, the isotopic ratios of our samples (around 1.1955 for $^{206}\text{Pb}/^{207}\text{Pb}$) fall within the range of values for Pacific mineral aerosols (Jones *et al.*, 2000) and natural sources in China (Lee *et al.*, 2007). They are obviously separated from the values of the anthropogenic emissions from near metropolises like Shanghai and Nanjing. In addition, it is worthy to note that the Pb isotopic ratios are quite similar to the signatures in the surface sediment of the Yangtze River (Choi *et al.*, 2007; Zhang *et al.*, 2008). Therefore, it is probably the natural, geogenic sources from the lands in China that mainly contribute to the Pb enrichment in the sediment of Yancheng coastal wetland. However, the anthropogenic pollution contribution can not be neglected in this region which is one of the most contaminated regions with concentrated population and developed industries in China (Fig. 10). In fact, the response of Pb isotopic ratios in the study area to the ban on use of leaded gasoline in China since 2000 is clear (Fig. 9b). We think the possible reason is that the fractions of anthropogenic Pb isotopic signatures have likely migrated and transformed during the water transportation. This transportation pathway is verified by the overlapping of the isotopic ratios in our sediments with the water samples of Nanjing (Luo *et al.*, 2014). Previous studies have indicated that anthropogenic Pb is rather mobile and exchangeable in the reducible fraction (Ettler *et al.*, 2011). In our study, the significant correlations between Pb and Fe/Mn (Fig. 7) were

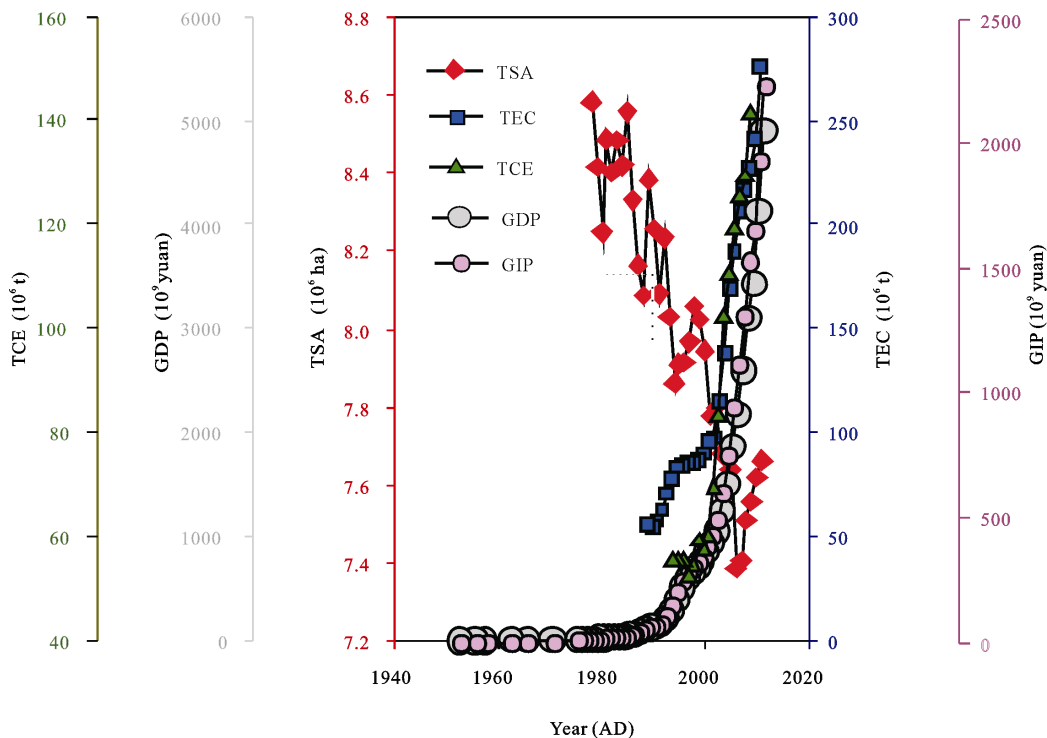


Fig. 10 Historical variations of social and economic development indicators in Jiangsu Province including gross domestic product (GDP), gross industrial production (GIP), total energy consumption (TEC) and total sown area (TSA) (Jiangsu Provincial Bureau of Statistics, 2013) and total carbon emission (TCE, 1995–2010) (Song *et al.*, 2015)

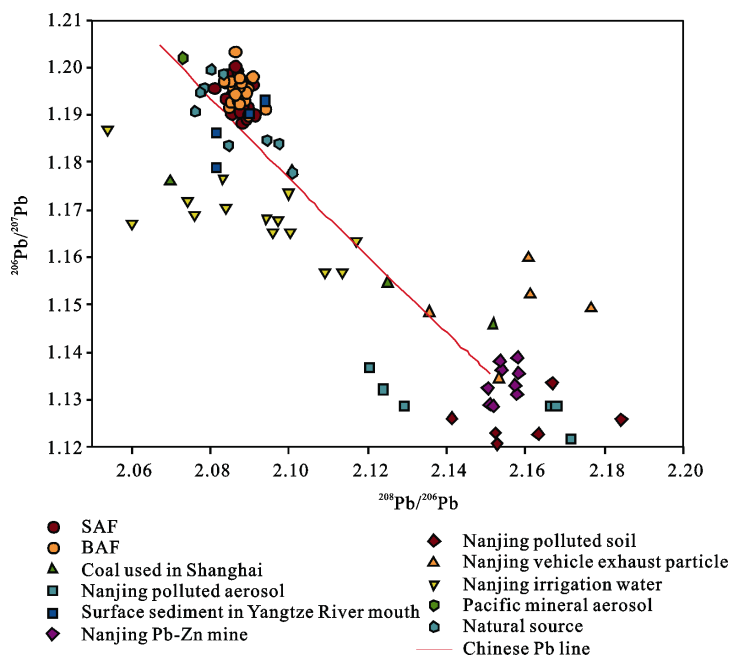


Fig. 11 Three isotopes plot ($^{206}\text{Pb}/^{207}\text{Pb}$ versus $^{208}\text{Pb}/^{206}\text{Pb}$) diagram for two cores from Yancheng coastal wetland, China. Values of possible Pb sources (coal used in Shanghai (Zheng *et al.*, 2004), polluted aerosol, water and soil, vehicle exhaust particles, and Pb-Zn mine in Nanjing (Luo *et al.*, 2014), natural source in China (Lee *et al.*, 2007), Pacific mineral aerosols (Jones *et al.*, 2000), and surface sediment in Yangtze River (Choi *et al.*, 2007; Zhang *et al.*, 2008)) are shown. The Chinese lead line was drawn based on the data for major lead mines in China (Mukai *et al.*, 2001)

found and the Fe-Mn oxides and oxyhydroxides may have masked the anthropogenic Pb isotopic signature (Bayon *et al.*, 2004).

5 Conclusions

We studied two intact ^{210}Pb -dated sediment cores from Yancheng coastal wetland in Jiangsu Province of East China and reconstructed the historical trend of Pb fluxes over the past 150 years, from the preindustrial to the modern period. The average Pb contents were 17.17–22.79 mg/kg and average Pb fluxes were 95.59–123.41 mg/(m²·yr). Although the Pb levels were still within the range of those of good quality soils in China, both enrichment factors (Pb EF) and accumulation rates (Pb AR) suggest an enhancing trend of Pb deposition in the sediment since 1860, which coincides with the sharp rise in energy consumption and industrial emission in recent decades. This reconstruction may therefore be helpful in informing the decision-making process related to policies for sustainable development.

Lead isotopic variability throughout the cores was small, with $^{206}\text{Pb}/^{207}\text{Pb}$ varying between 1.1883 and 1.2180, and $^{208}\text{Pb}/^{206}\text{Pb}$ varying between 2.0810 and 2.0940. Temporal variations in the potential natural and/or anthropogenic Pb sources were assessed based on the isotopic ratio and the 1/Pb ratio of the sediment samples and other end members from previous studies. Our results suggest that Pb input throughout the past 150 years was governed by water transportation from natural sources in the lands. However, the anthropogenic Pb input can not be ignored because the variation of $^{206}\text{Pb}/^{207}\text{Pb}$ since ca. 2003 exhibits an obvious response to banning the use of leaded gasoline in China in 2000. This may confirm that anthropogenic Pb is rather mobile and exchangeable in sediments with high Fe/Mn oxides and oxyhydroxides.

Acknowledgements

We would like to thank Drs. Cheng Rong and Sun Weiwei (Nanjing Institute of Geography and Limnology, Chinese Academy of Sciences) for their help in the field, and Mr. Zhu Yuxin and Mr. Xia Weilan for their help in the laboratory. Our sincere thanks are also extended to Dr. Neil McLaughlin (Agriculture and Agri-Food Canada) who provided excellent language polishing to im-

prove the text.

References

- Appleby P G, 2008. Three decades of dating recent sediments by fallout radionuclides: a review. *Holocene*, 18(1): 83–93. doi: 10.1177/0959683607085598
- Baldwin B, Butler C, 1985. Compaction curves. *American Association of Petroleum Geologists Bulletin*, 69(4): 622–626.
- Bao K, Xia W, Lu X *et al.*, 2010. Recent atmospheric lead deposition recorded in an ombrotrophic peat bog of Great Hinggan Mountains, Northeast China, from ^{210}Pb and ^{137}Cs dating. *Journal of Environmental Radioactivity*, 101: 773–779. doi: 10.1016/j.jenvrad.2010.05.004
- Bao K, Shen J, Wang G *et al.*, 2015a. Anthropogenic black carbon emission increase during the last 150 years at coastal Jiangsu, China. *PLoS ONE*, 10(7): e0129680. doi: 10.1371/journal.pone.0129680
- Bao K, Shen J, Sapkota A, 2015b. High-resolution enrichment of trace metals in a west coastal wetland of the southern Yellow Sea over the last 150 years. *Journal of Geochemical Exploration*, doi: http://dx.doi.org/10.1016/j.gexplo.2015.09.010
- Bayon G, German C, Burton K *et al.*, 2004. Sedimentary Fe-Mn oxyhydroxides as paleoceanographic archives and the role of aeolian flux in regulating oceanic dissolved REE. *Earth and Planetary Science Letter*, 224(3): 477–492. doi: 10.1016/j.epsl.2004.05.033
- Chan L, Ng S, Davis A *et al.*, 2001. Magnetic properties and heavy-metal contents of contaminated seabed sediments of Penny's Bay, Hong Kong. *Marine Pollution Bulletin*, 42(7): 569–583.
- Cheng H, Hu Y, 2010. Lead (Pb) isotopic fingerprinting and its applications in lead pollution studies in China: a review. *Environmental Pollution*, 158: 1134–1146. doi: 10.1016/j.envpol.2009.12.028
- Choi M S, Yi H I, Yang S Y *et al.*, 2007. Identification of Pb sources in Yellow Sea sediments using stable Pb isotope ratios. *Marine Chemistry*, 107(2): 255–274. doi: 10.1016/j.marchem.2007.07.008
- Chuai X, Huang X, Wang W *et al.*, 2014. Spatial simulation of land use based on terrestrial ecosystem carbon storage in coastal Jiangsu, China. *Scientific Report*, 4: 5667. doi: 10.1038/srep05667
- Church T M, Lord III C J, Somayajulu B, 1981. Uranium, thorium and lead nuclides in a Delaware salt marsh sediment. *Estuarine Coastal and Shelf Science*, 13(3): 267–275. doi: 10.1016/S0302-3524(81)80025-4
- Connor S E, Thomas I, 2003. Sediments as archives of industrialisation: evidence of atmospheric pollution in coastal wetlands of southern Sydney, Australia. *Water Air Soil and Pollution*, 149(1): 189–210. doi: 10.1023/A:1025626104164
- Deely J M, Fergusson J E, 1994. Heavy metal and organic matter concentrations and distributions in dated sediments of a small estuary adjacent to a small urban area. *Science of the Total En-*

- vironment*, 153(1): 97–111. doi: 10.1016/0048-9697(94)90106-6
- DeLaune R, Patrick W, Buresh R, 1978. Sedimentation rates determined by ^{137}Cs dating in a rapidly accreting salt marsh. *Nature*, 275: 532–533. doi: 10.1038/275532a0
- Di Leonardo R, Adelfio G, Bellanca A *et al.*, 2014. Analysis and assessment of trace element contamination in offshore sediments of the Augusta Bay (SE Sicily): A multivariate statistical approach based on canonical correlation analysis and mixture density estimation approach. *Journal of Sea Research*, 85: 428–442. doi: 10.1016/j.seares.2013.07.015
- Ettler V, Mihaljević M, Kribek B *et al.*, 2011. Tracing the spatial distribution and mobility of metal/metalloid contaminants in Oxisols in the vicinity of the Nkana copper smelter, Copperbelt province, Zambia. *Geoderma*, 164(1): 73–84. doi: 10.1016/j.geoderma.2011.05.014
- Fang S B, Xu C, Jia X B *et al.*, 2010. Using heavy metals to detect the human disturbances spatial scale on Chinese Yellow Sea coasts with an integrated analysis. *Journal of Hazard Material*, 184(1): 375–385. doi: 10.1016/j.jhazmat.2010.08.046
- Flegel A R, Gallon C, Ganguli P M, *et al.*, 2013. All the lead in China. *Critical Reviews in Environmental Science and Technology*, 43(7): 1869–1944. doi: 10.1080/10643389.2012.671738
- Gao J, Bai F, Yang Y *et al.*, 2012. Influence of *Spartina* colonization on the supply and accumulation of organic carbon in tidal salt marshes of northern Jiangsu province, China. *Journal of Coastal Research*, 28(2): 486–498. doi: 10.2112/JCOASTRES-D-11-00062.1
- Gao S, Du Y, Xie W *et al.*, 2014. Environment-ecosystem dynamic processes of *Spartina alterniflora* salt-marshes along the eastern China coastlines. *Science. China-Earth Science*, 57(11): 2567–2586. doi: 10.1007/s11430-014-4954-9
- GB15618–1995, 1997. *Environmental Quality Standard for Soils in China*. Beijing: Standards Press of China. (in Chinese)
- Hosono T, Su C C, Siringan F *et al.*, 2010. Effects of environmental regulations on heavy metal pollution decline in core sediments from Manila Bay. *Marine Pollution Bulletin*, 60(5): 780–785. doi: 10.1016/j.marpolbul.2010.03.005
- Jayaprakash M, Urban B, Velmurugan P *et al.*, 2010. Accumulation of total trace metals due to rapid urbanization in microtidal zone of Pallikarai marsh, south of Chennai, India. *Environmental Monitoring and Assessment*, 170(1): 609–629. doi: 10.1007/s10661-009-1261-6
- Jiangsu Provincial Bureau of Statistics, 2013. *Jiangsu Statistical Yearbook*. Beijing: China Statistics Press. (in Chinese)
- Jones C E, Halliday A N, Rea D K *et al.*, 2000. Eolian inputs of lead to the North Pacific. *Geochimica et Cosmochimica Acta*, 64(8): 1405–1416. doi: 10.1016/S0016-7037(99)00439-1
- Kapička A, Petrovský E, Ustjak S *et al.*, 1999. Proxy mapping of fly-ash pollution of soils around a coal-burning power plant: a case study in the Czech Republic. *Journal of Geochemical Exploration*, 66(1): 291–297. doi: 10.1016/S0375-6742(99)00008-4
- Ke C, Zhang D, Wang F *et al.*, 2011. Analyzing coastal wetland change in the Yancheng National Nature Reserve, China. *Regional Environmental Change*, 11(1): 161–173. doi: 10.1007/s10113-010-0130-8
- Kim G, Alleman L, Church T, 2004. Accumulation records of radionuclides and trace metals in two contrasting Delaware salt marshes. *Marine Chemistry*, 87(3): 87–96. doi: 10.1016/j.marchem.2004.02.002
- Kim G, Hussain N, Church T M *et al.*, 1997. The fallout isotope ^{207}Bi in a Delaware salt marsh: a comparison with ^{210}Pb and ^{137}Cs as a geochronological tool. *Science of the Total Environment*, 196(1): 31–41. doi: 10.1016/S0048-9697(96)05385-5
- Kirwan M L, Megonigal J P, 2013. Tidal wetland stability in the face of human impacts and sea-level rise. *Nature*, 504: 53–60. doi: 10.1038/nature12856
- Lee C S, Li X D, Zhang G *et al.*, 2007. Heavy metals and Pb isotopic composition of aerosols in urban and suburban areas of Hong Kong and Guangzhou, South China—evidence of the long-range transport of air contaminants. *Atmospheric Environment*, 41(2): 432–447. doi: 10.1016/j.atmosenv.2006.07.035
- Leorri E, Cearreta A, García-Artola A *et al.*, 2013. Relative sea-level rise in the Basque coast (N Spain): Different environmental consequences on the coastal area. *Ocean and Coastal Management*, 77: 3–13. doi: 10.1016/j.ocecoaman.2012.02.007
- Li J, Gao S, 2013. Estimating deposition rates using a morphological proxy of *Spartina alterniflora* plants. *Journal of Coastal Research*, 29(6): 1452–1463. doi: http://dx.doi.org/10.2112/JCOASTRES-D-12-00186.1
- Li Q, Cheng H, Zhou T *et al.*, 2012. The estimated atmospheric lead emissions in China, 1990–2009. *Atmospheric Environment*, 60: 1–8. doi: 10.1016/j.atmosenv.2012.06.025
- Liu Z, Pan S, Liu X *et al.*, 2010. Distribution of Cs-137 and Pb-210 in sediments of tidal flats in north Jiangsu Province. *Journal of Geographical Science*, 20(1): 91–108. doi: 10.1007/s11442-010-0091-3
- Liu Z, Pan S, Yin Y *et al.*, 2013. Reconstruction of the historical deposition environment from ^{210}Pb and ^{137}Cs records at two tidal flats in China. *Ecological Engineer*, 61(Part A): 303–315. doi: 10.1016/j.ecoleng.2013.09.029
- Luo L, Chu, B, Liu Y *et al.*, 2014. Distribution, origin, and transformation of metal and metalloid pollution in vegetable fields, irrigation water, and aerosols near a Pb-Zn mine. *Environmental Science and Pollution Research*, 21(13): 8242–8260. doi: 10.1007/s11356-014-2744-8
- Mahiques M M, Figueira R C L, Salaroli A B *et al.*, 2013. 150 years of anthropogenic metal input in a biosphere reserve: The case study of the Cananéia-Iguaçu coastal system, southeastern Brazil. *Environmental Earth Science*, 68(4): 1073–1087. doi: 10.1007/s12665-012-1809-6
- Mihaljević M, Zuna M, Ettler V *et al.*, 2006. Lead fluxes, isotopic and concentration profiles in a peat deposit near a lead smelter (Příbram, Czech Republic). *Science of the Total Environment*, 372(1): 334–344. doi: 10.1016/j.scitotenv.2006.09.019
- Molisani M, Marins R, Machado W *et al.*, 2004. Environmental changes in Sepetiba Bay, SE Brazil. *Regional Environmental*

- Change*, 4(1): 17–27. doi: 10.1007/s10113-003-0060-9
- Monteiro F F, Cordeiro R C, Santelli R E et al., 2012. Sedimentary geochemical record of historical anthropogenic activities affecting Guanabara Bay (Brazil) environmental quality. *Environmental Earth Science*, 65(6): 1661–1669. doi: 10.1007/s12665-011-1143-4
- Mukai H, Tanaka A, Fujii T et al., 2001. Regional characteristics of sulfur and lead isotope ratios in the atmosphere at several Chinese urban sites. *Environmental Science and Technology*, 35(6): 1064–1071. doi: 10.1021/es001399u
- Patterson C, Settle D, 1987. Review of data on eolian fluxes of industrial and natural lead to the lands and seas in remote regions on a global scale. *Marine Chemistry*, 22(2): 137–162. doi: 10.1016/0304-4203(87)90005-3
- Pennings S C, 2012. The big picture of marsh loss. *Nature*, 490: 352–353. doi: 10.1038/490352a
- Perillo G, Wolanski E, Cahoon D et al., 2009. *Coastal Wetlands: An Integrated Ecosystem Approach*. Amsterdam: The Netherlands: Elsevier, pp. 974.
- Perkins S M, Filippelli G M, Souch C J, 2000. Airborne trace metal contamination of wetland sediments at Indiana Dunes National Lakeshore. *Water Air and Soil Pollution*, 122(1): 231–260. doi: 10.1023/A:1005254916966
- Qiu J, 2011. China faces up to 'terrible' state of its ecosystems. *Nature*, 471: 19–19. doi: 10.1038/471019a
- Regnier P, Friedlingstein P, Ciais P et al., 2013. Anthropogenic perturbation of the carbon fluxes from land to ocean. *Nature Geoscience*, 6: 597–607. doi: 10.1038/ngeo1830
- Sharma P, Gardner L, Moore W et al., 1987. Sedimentation and bioturbation in a salt marsh as revealed by ^{210}Pb , ^{137}Cs , and ^7Be studies. *Limnology and Oceanography*, 32(2): 313–326. doi: 10.4319/lo.1987.32.2.0313
- Song M, Guo X, Wu K et al., 2015. Driving effect analysis of energy-consumption carbon emissions in the Yangtze River Delta region. *Journal of Cleaner Production*, 103: 620–628. doi: 10.1016/j.jclepro.2014.05.095
- SPSS, 2002. *Statistical Product and Service Solution*, version 11.5. Chicago, IL, USA: SPSS Inc.
- Wang Aijun, Gao Shu, Jia Jianjun et al., 2005. Contemporary sedimentation rates on salt marshes at Wanggang, Jiangsu, China. *Acta Geographica Sinica*, 60(1): 61–70. (in Chinese)
- Wang D, Zhao Z, Dai M, 2014. Tracing the recently increasing anthropogenic Pb inputs into the East China Sea shelf sediments using Pb isotopic analysis. *Marine Pollution Bulletin*, 79(1): 333–337. doi: 10.1016/j.marpolbul.2013.11.032
- Zhang W, Feng H, Chang J et al., 2008. Lead (Pb) isotopes as a tracer of Pb origin in Yangtze River intertidal zone. *Chemical Geology*, 257(3): 257–263. doi: 10.1016/j.chemgeo.2008.10.012
- Zheng J, Tan M, Shibata Y et al., 2004. Characteristics of lead isotope ratios and elemental concentrations in PM10 fraction of airborne particulate matter in Shanghai after the phase-out of leaded gasoline. *Atmospheric Environment*, 38(8): 1191–1200. doi: 10.1016/j.atmosenv.2003.11.004
- Zohar I, Bookman R, Teutsch N et al., 2014. The contamination history of lead and other trace metals reconstructed from an urban winter pond in the Eastern Mediterranean coast (Israel). *Environmental Science and Technology*, 48(23): 13592–13600. doi: 10.1021/es500530x
- Zourarah B, Maanan M, Carruesco C et al., 2007. Fifty-year sedimentary record of heavy metal pollution in the lagoon of Oualidia (Moroccan Atlantic coast). *Estuarine Coastal and Shelf Science*, 72(1): 359–369. doi: 10.1016/j.ecss.2006.11.007
- Zwolsman J J, Berger G, Van Eck G, 1993. Sediment accumulation rates, historical input, postdepositional mobility and retention of major elements and trace metals in salt marsh sediments of the Scheldt estuary, SW Netherlands. *Marine Chemistry*, 44(1): 73–94. doi: 10.1016/0304-4203(93) 90007-B